CrossMark

ORIGINAL CONTRIBUTION

Investigation of water-based and oil-based ferrofluids with a new magnetorheological cell: effect of the microstructure

Cécilia Galindo-Gonzalez[1] · Alain Ponton[1] · Agnes Bee[2] · Jean Chevalet[2] ·
Delphine Talbot[2] · Regine Perzynski[2] · Emmanuelle Dubois[2]

Abstract A new magnetorheological cell is implemented to perform measurements of temperature-controlled flows and determine viscoelastic properties in magnetic complex fluids under applied continuous magnetic fields. The flow properties of water-based and oil-based ferrofluids with volume fractions up to 10 % are investigated here in various situations of interparticle interaction, leading also to various microstructures already known from previous works. Shear flow behaviors under magnetic fields resulting in a competition between magnetic and hydrodynamic forces are directly related to the microscopic structure of the probed magnetic fluids.

Keywords Magnetic fluids · Nanoparticles · Magnetorheology · Flow behavior · Yield stress · Microstructure

Introduction

Ferrofluids (FFs) are colloidal dispersions of magnetic nanoparticles (nanomagnets) in a solvent. They are materials that spontaneously flow towards regions of large magnetic field. Thanks to their magnetic properties and their behaviors under applied magnetic field, they have numerous applications from industrial devices such as magnetic seals, magnetocaloric

✉ Alain Ponton
alain.ponton@univ-paris-diderot.fr

[1] Laboratory MSC, UMR 7057, Univ Paris Diderot-Paris 7, CNRS, Bât. Condorcet, CC 7056, 75205 Paris Cedex 13, France

[2] Sorbonne Universités, UPMC Univ Paris 06, UMR 8234, PHENIX, F-75005 Paris, France

cooling systems, or assisted dampers, to biomedical issues of paramount importance (Arias et al. 2005; Duran et al. 2008; Gomez-Lopera et al. 2006). For most of these applications, the rheological behavior under field is a crucial point that must be known and controlled. It is tightly connected to the local structure of the magnetic fluid under field, which can be monophasic or diphasic on the microscale (Cousin et al. 2003; Dubois et al. 2000; Mertelj et al. 2009; Shima and Philip 2011). On the nanoscale, this local structure can be that of a liquid with individual nanoparticles (Mériguet et al. 2006; Wandersman et al. 2009a) or with aggregates (Itri et al. 2001; Frka-Petesic et al. 2013). The associated rheological behavior may thus be that of a fluid, Newtonian or not, but it may also be that of a thixotropic gel (Hasmonay et al. 1999) or of a ferroglass (Wandersman et al. 2009b). More complex smart magnetic systems may be obtained by introducing non-magnetic objects inside the ferrofluid such as polymeric chains (Galicia et al. 2009), micelles (Patel 2011) or non magnetic clay nanoplatelets (Cousin et al. 2002; Galindo-Gonzalez et al. 2005), producing also non-Newtonian effects. Note that we are not interested here in the general class of the so-called magnetorheological fluids usually based on micron-sized beads which customarily behave as solids under field with very large yield stresses (Park et al. 2010; Vicente et al. 2011). We focus here on nanosize magnetic particles. Many efforts have been dedicated to the study of the effect of the external magnetic fields on the rheological properties of the magnetic fluids and to the development or adaptation of devices to apply magnetic field during the rheological measurements. Let us begin with a short review of these various devices. Some authors employed for ferrofluids a pressurized capillary rheometer in which the magnetic field is applied with two parallel permanent magnets surrounding the whole capillary, producing a field perpendicular to the capillary to study ferrofluids (Ren et al. 2008). Brookfield rotational rheometers have been also used under field (Hong et al. 2007, 2009). Such

devices are only useful with Newtonian fluids, a point which strongly limits their applications.

To overcome these limitations, Odenbach et al. have designed a special rheometer for magnetic fluids with a cone and plate arrangement (Odenbach et al. 1999), which enables the study of magnetoviscoelastic behaviors. It has been used for the study of commercial FFs (Borin and Odenbach 2009; Odenbach and Stork 1998; Odenbach et al. 1999; Zubarev et al. 2002) and home-made FFs (Borin and Odenbach 2009; Kroell et al. 2005). The main limitation of this device is that it is a strain rate-controlled rheometer which does not allow the direct measurement of the yield stress and its evolution with field. Therefore, they have also developed a stress-controlled rheometer (Shahnazian and Odenbach 2007, 2008a) with which various ferrofluids have been probed (Shahnazian and Odenbach 2007, 2008b; Shahnazian et al. 2009). In this device designed for ferrofluids, the torque is transmitted by a fluid coupling with a limited stress range. Moreover the magnetic field is produced by one coil surrounding the cone and plate geometry which cannot allow an easy insertion and/or visualization of the sample.

The commercial system MCR of Anton Paar has also been used in several studies on ferrofluids (Rodriguez-Arco et al. 2011). In this device, the magnetic field is applied by means of a coil placed below the bottom plate of the rheometer. It has however several serious restrictions: the difficulty to control the true applied magnetic field, its poor homogeneity, and the sensitivity of the rheometer being limited to systems with high enough viscosities, and not too small shear stresses (above 3 Pa, see for example (Galindo-Gonzalez et al. 2012)). Thus, this kind of device is much more suited for magnetorheological fluids (MRF) (Lopez-Lopez et al. 2008; Vereda et al. 2011), which are suspensions of micrometric particles, than for classic ferrofluids, in water for example. Indeed, the multidomain particles of MRF, which have a zero magnetic moment without field, become strongly magnetic under a field and form chains and columns. It induces huge rheological modifications with a transition from a viscous liquid to a solid-like behavior. The ranges of viscosities and implied stresses are completely different from those which are needed for the study of ferrofluids based on nanoscaled particles. For MRF, several authors have adapted rheometers, for example, with Helmholtz coils placed with their axes coinciding with the rotational axis of the vane tool in a Bohlin CS10 which provides very weak fields ($H = 1.6$ kA/m) (Lopez-Lopez et al. 2006) or by means of a solenoid placed around the measuring geometry in a Thermo Haake RS150 rheometer (Gomez-Ramirez et al. 2011; Kuzhir et al. 2011) which does not allow any observation of the sample.

In this context, our aim here is to develop a magnetorheological cell to measure temperature-controlled flow and viscoelastic properties under applied continuous magnetic field of magnetic dispersions. They are, here

ferrofluids, based on nanoparticles dispersed in water or in an organic solvent with a well-controlled structure before turning us towards the study of more complex systems. The specifications of the device are the following: (i) ability to measure viscosities down to the one of water, (ii) ability to measure viscoelastic properties, (iii) ability to apply a controlled stress, (iv) homogeneity and good control of the magnetic field applied to the sample, (v) ability to fill the cell and to perform experiments (or series of experiments) under controlled atmosphere, and (vi) ability to maintain the sample in the working area at a temperature accurately stabilized given, at least, the influence of the dissipation of the field coils. Such a magnetorheometer combining all these characteristics has never been described in the literature and cannot be bought. Such a device has been thus designed and built, implementing most of these specifications.

The system is used here for an investigation on home-made ferrofluid samples whose structure has already been tested previously by several techniques on complementary spatial scales, among which small-angle neutron and X-ray scattering (Mériguet et al. 2012). It allows us to directly correlate the finely tuned state of interparticle interaction and the microscopic structure to the rheological behavior as well as to determine the sensitivity of our device.

Magnetic fluids: preparation and characteristics

Preparation of the magnetic fluids

The magnetic fluids studied here are all based on home-made samples with controlled compositions, which allows us to modify and tune the interparticle potential and thus to control the microstructure (Cousin et al. 2003; Dubois et al. 2000; Gazeau et al. 2003; Hasmonay et al. 1999; Mériguet et al. 2006, 2012). The preparation of the particles and their dispersion are described in the following as well as the different techniques that allow us to obtain their characteristics given in Table 1.

The two basic steps to obtain the ferrofluids are the synthesis of the nanoparticles and their dispersion in a liquid carrier with an appropriate treatment of the surface. Experimental methods detailed in (Bee et al. 1995; Dubois et al. 1999; Massart 1980, 1981; Mériguet et al. 2003; Tourinho et al. 1990) are briefly explained below.

Synthesis of the nanoparticles NPs

Maghemite (γ-Fe$_2$O$_3$) nanoparticles are prepared by alkaline coprecipitation of ferric and ferrous salts in water (Massart 1980, 1981). Concentrated ammonium hydroxide is added to an acidic solution of iron (II) chloride and iron (III) chloride leading to the precipitation of anionic magnetite (Fe$_3$O$_4$) particles. After washing with distilled water, they are stirred in

Table 1 Magnetic fluids and their characteristics

Particles	Ψ_{dd}	Ferrite	Samples	Surface ligands	Solvent	Free species (mol/L)	Volume fraction	d_H (nm)	State	Diffraction under field
A	36	Fe	A_{acid}	Hydroxo	Water pH ~ 2	0.03	3.47 %	23 ± 1	Sol of NPs	Weak
			A_{cit}	Citrate	Water pH ~ 7	0.013	3.47 %	23 ± 1	Sol of NPs	Weak
B	29	Fe	Series B	Hydroxo	Water		1.5 %	21 ± 1		
			B0 to B2		2 ≤ pH ≤ 2.5	~0.05			Sol of NPs	Weak
			B3 to B6		2.6 ≤ pH ≤ 3.3	~0.05			Sol of clusters	Yes
			B7 to B12		3.5 ≤ pH ≤ 4.2	~0.05			Gels	Yes
C	29	Fe	Series C	Citrate	Water pH ~ 7			18 ± 1		
			C0			0.017	1.6 %		Sol of NPs	Weak
			C1			0.008	3.9 %		Sol of NPs	Weak
D	33	Co	D	Citrate	Water pH ~ 7	0.028	1.3 %	20 ± 1	Sol of NPs	No
			D_G	Citrate	Glycerine	0.028	1.6 %	20 ± 1	Sol of NPs	No
F	30	Fe	F	BNE	Silicone oil	–	4.2 %	27 ± 1	Sol of NPs	No
G	21	Fe	G	BNE	Dibutyl phtalate	–	11.6 %	–	Sol of NPs	No

Particles: name of the particles constituting the samples; Ψ_{dd}: magnetic dipolar parameter characterizing the particles (see text for formula); ferrite constituting the nanoparticles: Fe = γ-Fe$_2$O$_3$, Co = CoFe$_2$O$_4$; surface ligands: nature of the species or groups on the surface of the nanoparticles, solvent: nature and the pH in the case of water; volume fraction of magnetic material in the samples; free species: concentration of these species in the solvent, i.e., sodium citrate for samples at pH ≃ 7 and nitric acid for acidic samples; state: structure of the samples (sols of nanoparticles (sols of NPs) or of clusters, or gels which are thixotropic); d_H (nm): hydrodynamic diameter determined from dynamic light scattering; diffraction under field indicates if diffraction is observed under a magnetic field H = 400 Oe = 32 kA/m, thus if samples remain homogeneous on the micron scale under field (see text for details)

nitric acid, oxidized into maghemite (γ-Fe$_2$O$_3$) by a boiling solution of ferric nitrate, and washed with acetone. These nanoparticles coated with hydroxo ligands are spontaneously soluble in aqueous acidic solutions at pH ~2 with NO$_3^-$ counterions (and in alkaline media with TMA$^+$ counterions (Bacri et al. 1990) (case of samples A$_{acid}$ and B in Table 1). The size distribution at the end of the synthesis is rather large (polydispersity index of a log-normal distribution of diameters of the order of 0.4). Several strategies may be developed to reduce this size distribution by centrifugation to eliminate the largest aggregates or by fractional precipitation taking advantage of the phase separation in two liquid phases which is obtained at large ionic strength (Dubois et al. 1999; Bacri et al. 1989). Cobalt ferrite (CoFe$_2$O$_4$) nanoparticles are prepared by coprecipitating acidic aqueous solutions of Co(NO$_3$)$_2$-FeCl$_3$ mixtures in alkaline medium at 100 °C (Bee et al. 1995; Tourinho et al. 1990). Washing steps with water are also performed. As these cobalt ferrite nanoparticles, coated at this step with hydroxo ligands, are not chemically stable in acid solutions in the long term, they are shortly treated with nitric acid before modification of their surface as will be explained here under.

Tuning of the particles surface and dispersion

As already said above, the particles at the end of the synthesis can be directly dispersed in an acidic HNO$_3$ solution.

Exchanging the hydroxo ligands coating the surface of the native particles (Bacri et al. 1990; Cruz et al. 2005; Dubois et al. 1999; Mériguet et al. 2003) by various surface ligands allows us to produce stable dispersions in various other solvents.

Firstly in water, the surface can be coated with citrate ligands in order to obtain dispersions at pH ~7. This coating is obtained by adding trisodium citrate to the native acidic ferrofluid ([Cit]/[iron] = 0.1), which is heated at 90 °C during 10 min (Dubois et al. 1999). After several washings with water/acetone mixtures, a stable citrated ferrofluid with pH close to 7 is obtained. The ionic strength, due to the free sodium citrate in the solution and the pH can be adjusted by dialysis (case of sample C in Table 1). Note that this coating is used for cobalt ferrite nanoparticles in order to obtain chemically stable dispersions on the long term in water at pH 7 (case of sample D in Table 1). This coating is also used for the dispersions in glycerine or water/glycerine mixtures. Glycerine is added in the aqueous ferrofluid, water being then removed by evaporation, totally or partially (case of sample D$_G$ in Table 1).

In order to stabilize the nanoparticles in organic solvents, they are coated with a surfactant, here commercial BNE (Beycostat NE), frequently used as surface ligand (Bacri et al. 1990). It is an anionic surfactant composed of a mixture of mono- and diesters of phosphoric acid, the chain being an alkylphenol containing nine ethoxy groups.

To produce the dispersions in silicone oil, BNE (2 g) is added to an acidic ferrofluid based on maghemite nanoparticles (50 mmol of iron) and the mixture is heated to 50 °C. The nanoparticles becoming hydrophobic, they flocculate. After several washings of the precipitate with methanol, the particles are dispersed in silicone oil (rhodorsil 763) as in (Cruz et al. 2005) (case of sample F in Table 1).

To produce the dispersions in dibutyl phtalate (DBP), BNE is added in the ferrofluid with the ratio 41 mg BNE/mmol of iron and the nitric acid concentration is increased by 0.15 mol/L by adding concentrated nitric acid (65 %). After heating the mixture at 50 °C under stirring during 10 min, the supernatant is removed after decantation and replaced by a smaller volume of water (five times less). After this step, when the DBP is added, there is a phase transfer of the particles towards DBP and the final ferrofluid concentration is simply controlled by the ratio of the volume of aqueous ferrofluid used at the beginning to the added volume of DBP. The quantity of BNE is the minimum necessary to get a full phase transfer with a minimum of unused surfactant (Mériguet et al. 2003). This method allows us to directly get the desired volume fraction (case of sample G in Table 1).

Characteristics of the magnetic fluids

The properties of the dispersions, in particular their microstructure, are controlled by several parameters which are determined for each dispersion. The methods are shortly explained hereunder.

NPs volume fraction

The volume fraction Φ of the magnetic fluids is calculated from chemical determinations of the metallic species by atomic absorption spectroscopy (Perkin Elmer Analyst 100) after dissolution of the particles in hydrochloric acid, using the molecular weight of the NP material (160 g/mol for maghemite and 235 g/mol for cobalt ferrite) and its density (5 g/cm^3 for maghemite and 5.29 g/cm^3 for cobalt ferrite). Note that in the case of NPs dispersed in apolar solvents and stabilized by surfactant coating, this volume fraction Φ does not take into account the volume of absorbed layer in the surface of the particles.

NPs superficial charge and free ionic species in the polar solvents

The NPs surface charge and concentration of free ionic species are essential parameters in aqueous ferrofluids as they control the electrostatic interactions between particles and the ferrofluid local structure (Mériguet et al. 2012). The ionic strength of the dispersion is linked to the concentration of free ions in the solution and to their valence.

In acidic ferrofluids, the NPs charge is positive and results from hydroxo groups on their surface. The counterions are nitrate. This charge, which is maximal at pH = 2 and equal 0.2 C/m^2 can be progressively decreased to 0.1 at pH ~4 and to zero at pH = 7, particles being then flocculated (Bacri et al. 1990). The ionic strength is due to H_3O^+ and NO_3^- ions at pH = 2 and to H_3O^+, NO_3^-, and TMA^+ while increasing pH with TMAOH. Repulsive interparticle interaction can thus be tuned in this system by changing the NPs charge at almost constant ionic strength.

In the citrated ferrofluids, the NPs charge is ensured by citrate ions which are adsorbed on the oxide surface by means of hydroxo groups and part of carboxylate groups. Therefore, part of the carboxylates remains free and ensure a negative charge on the particle, compensated by sodium counterions, of equivalent concentration $[Na^+]_{part}$, which provides the value of the structural charge of the particles (Dubois et al. 1999). Adsorbed citrate molecules are in equilibrium with free trisodium citrates, the concentration of which is 1/3 of $[Na^+]_{free}$. Hence, the quantification of sodium, achieved by atomic absorption spectroscopy after dissolution of the maghemite particles by concentrated HCl, is the easiest way to determine the structural charge of the nanoparticles. Indeed, the total concentration of sodium ions $[Na^+]_{tot}$ in the ferrofluid equals the sum of $[Na^+]_{part}$ and $[Na^+]_{free}$. The structural charge is thus directly obtained from $[Na^+]_{part}$, measured after separation of the nanoparticles from the supernatant by centrifugation on a membrane or by difference of $[Na^+]_{tot}$ and $[Na^+]_{free}$. The maximal charge is 0.2 C/m^2 as in the acidic ferrofluids (Bacri et al. 1990; Gazeau et al. 2002); however, it is kept constant and the repulsive interparticle interaction can be tuned by changing the ionic strength (Mériguet et al. 2012).

NPs surfaces and free species in apolar solvents

In these systems, the surface of the nanoparticles is covered by surfactants and the quantity of free surfactant in the solvent is minimized by the preparation process (Mériguet et al. 2003). A detailed composition cannot be experimentally obtained here for such an industrial surfactant.

Structure in zero applied magnetic field

Firstly, the structure on the micron scale is obtained from optical microscopy. Biphasic sample where two phases coexist due to insufficient repulsion (low charge, high surfactant or ionic concentration) are easily ruled out (Bacri et al. 1990; Berkovski 1996; Cousin et al. 2003; Dubois et al. 2000; Sandre et al. 1999). For homogeneous monophasic dispersions, the local structure can be studied by small-angle scattering (SAS), either neutrons (SANS) or X-rays (SAXS). From previous studies on similar samples, we have shown that the structure can strongly vary with NP coatings, free

species, diameters, and solvent, and we therefore know the domains of the different types of structures (Dubois et al. 1999, 2000; Frka-Petesic et al. 2013; Mériguet et al. 2006, 2012).

Stability under a constant homogeneous magnetic field

A magnetic field H can induce a phase separation in a homogeneous dispersion as it increases the attractions on average. The easiest way to detect this phase separation is an optical measurement. The sample is put in an optical cell of thickness 100 μm and placed in a magnetic field H, static, and uniform, parallel to the cell. The sample cell is then illuminated perpendicularly to the walls (and thus to the field H) by a He-Ne laser beam and the diffracted intensity on the line perpendicular to the beam and to the direction of the field H is measured. No light is diffracted if the ferrofluid remains monophasic under field. On the contrary, a diffracted line perpendicular to the field is observed if the fluid separates in two phases (Bacri et al. 1990; Sandre et al. 1999). Indeed needles of a more concentrated phase are formed in the fluid, and their elongated shape diffracts the laser beam. The same is observed if microaggregates are formed as they are elongated along the field (Frka-Petesic 2010; Mériguet et al. 2012). This information is crucial as it indicates the microstructure of the fluids on the microscale under field. Here, we probe the samples under a constant homogeneous field between 0 and 80 kA/m (in a slightly larger range than the magnetic field strength applied in the rheometer). Note that, if the magnetic fluid is already diphasic in zero field, this phase separation is observed in very weak fields, of the order of 1 kA/m (Sandre et al. 1999) otherwise the diffraction line occurs around a few 10 kA/m.

Magnetic properties of the ferrofluids

The magnetic properties are determined by magnetization M measurements on stable dispersions under an applied magnetic field H, ranging here between 0 and 800 kA/m, at room temperature with a home-made vibrating magnetometer. An example is shown in Fig. 1 for sample A with a representative micrograph of nanoparticles obtained by transmission electron microcopy. Low-field measurements of M_{LF} in the linear-in-H region (see inset of Fig. 1) enable the determination of the initial magnetic susceptibility $\chi_0 = M_{LF}/H$. High field determination of M_{HF} in the saturation region allows us to determine the saturation magnetization M_S of the nanoparticles as $M_S = M_{HF}/\Phi$. In all samples here, the size distribution of NPs can be described by a log-normal distribution of diameters with the same median diameter $d_0 \sim 7$ nm (with $\ln d_0 = <\ln d>$) and a polydispersity index σ between 0.3 and 0.4 with a saturation magnetization $M_S = 310 \pm 25$ kA/m. These parameters are determined from the fit of the magnetization (measured in dilute fluids with negligible interparticle interactions) by a Langevin

formalism weighted by the size distribution (Berkovski 1996). However, as d_0 is constant here, polydispersity can also be finely quantified in terms of parameter $\Psi_{dd} = \mu_0 M^2_S V_{NP}/k_B T$, V_{NP} being a low-field averaged NPs magnetic volume. This Ψ_{dd} parameter quantifies the raw magnetic dipolar interaction between NPs at low Φ (Mériguet et al. 2012). It is determined from the low-field measurements: indeed in the Langevin limit $3\chi_0/\Phi = \Psi_{dd}$ (see values in Table 1). Note that the quantity $\lambda^* = \Psi_{dd}/24$ is frequently used in literature instead of Ψ_{dd}. Here, Ψ_{dd} is always smaller than 36 and λ^* always smaller than 1.5, meaning that there is no chaining of the nanoparticles in the samples at zero magnetic field (Huang et al. 2005).

Hydrodynamic diameter of the NPs

Another mean size of the particles can be determined by quasi-elastic light scattering (Zetasizer Nano ZS device (Malvern Instruments, UK)). A hydrodynamic diameter is determined, which is a high moment of the size distribution. This size determination is sensitive to the largest particles in the distribution, which produce a stronger scattering than the other ones, and a similar average is obtained by relaxation of magnetobirefringence in low fields (Bacri et al. 1987; Berkovski 1996). Due to strong light absorption of the ferrofluids, the measurements are performed on very dilute samples at $\Phi \sim 10^{-2}$ %. Note that this unavoidable dilution (not always possible) for QELS measurements may either destroy some aggregates or on the contrary produce new ones, depending on how the dilution is performed. Here the values of d_H are all around 20 nm which is consistent with the previous magnetic determinations in low field (see Table 1).

Interparticle interactions and microstructure

Table 1 gathers the information on all the studied samples with different kinds of interparticle potentials by controlling the following: (i) the nature of the material (maghemite (γ-Fe$_2$O$_3$) or cobalt ferrite (CoFe$_2$O$_4$)), (ii) the size distribution of the particles, thus magnetic dipolar and Van der Waals interactions, (iii) the volume fraction of particles, (iv) their surface coating thus the solid/liquid interface and the nature and strength of the repulsion, and (v) the solvent. Two natures (iron oxide and cobalt ferrite) of NPs are compared with a given particle size distribution (mean diameter $d_0 = 7$ nm, polydispersity being quantified by the parameter Ψ_{dd}) and different volume fractions. The stabilization of NPs depends on the nature of solvent as already extensively studied in our previous works [Cousin et al. 2003; Dubois et al. 2000; Gazeau et al. 2003; Hasmonay et al. 1999; Mériguet et al. 2006; Mériguet et al. 2012).

For the dispersions in apolar solvents (samples F and G in Table 1), with the commercial surfactant called BNE, good solvents of BNE are chosen and the minimal quantity of

Fig. 1 *Left*: magnetization curve for the fluid C at $\Phi = 0.33$ %; *dots* are the data and the low magnetic field region where the initial susceptibility can be determined. *Right*: transmission electron microcopy of maghemite nanoparticles
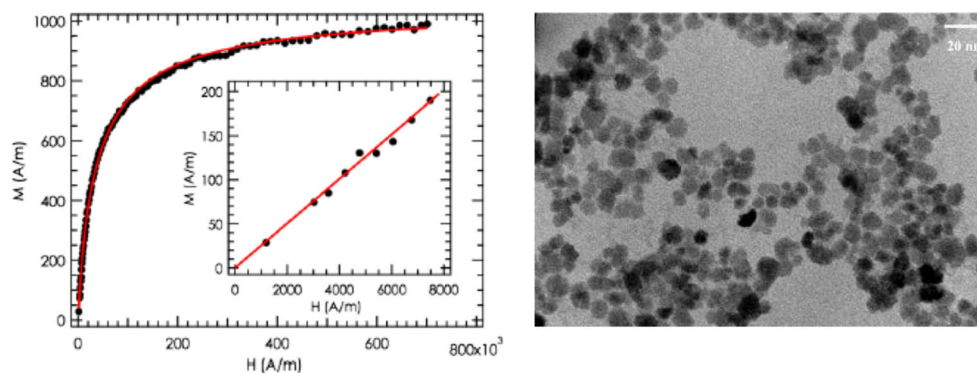
surfactant is used in order to reduce the amount of free surfactant in the dispersions. In these conditions, strong repulsions between particles are obtained, as proven by the low value of the structure factor S(Q) at low scattering vector Q, as determined from small-angle scattering (data not shown). For example, for sample G, we know from SAXS at low Q that the structure factor at Q = 0 is around 0.2. Moreover, these dispersions are perfectly stable under magnetic field.

In the dispersions in water with hydroxo surface ligands, interactions can be tuned from repulsive to attractive thanks to the variation with pH of the surface charge of the particles. It can be tuned from positive, with a zeta potential of the order of +30 mV (Lopes Filomeno—to be published), at pH = 2 to zero at pH = 7 with a quasi constant ionic strength (series B in Table 1, see details in Table 2). Samples from series B are prepared from B0 by addition of tetramethylammonium hydroxide (TMAOH); therefore, the free species are here TMANO₃. The charge is maximal at pH = 2 and the particles are well dispersed, as proven in Fig. 2a and b for two samples

at pH = 2, sample B0 and a similar one with structure factor at pH = 2 lower than 1 at low scattering vector Q—see Fig. 2b. When pH increases thus decreasing the surface charge at almost constant ionic strength (samples B3 to B12 in Tables 1 and 2), sols of clusters are formed due to weak attractions as shown by S(Q) larger than 1 at small Q (Fig. 2a, b at pH larger than 2), and they evolve towards thixotropic gels at higher pH (Mériguet et al. 2012; Frka-Petesic 2010). Similar samples have been already characterized in previous studies by magneto-optical and rheological measurements: loose clusters are formed with roughly 30 NPs per cluster, with a fractal dimension of the order of 2 (Frka-Petesic 2010; Hasmonay et al. 1999; Ponton et al. 2002, 2005).

In the dispersions in water with citrate ligands on the particles surface (biocompatible dispersions at pH = 7 with sodium citrate as free species), interactions can also be tuned from repulsive to attractive; however, here the structural charge of the particles remains constant while increasing the ionic strength. Among these systems, we focus here on repulsive samples with low enough free citrate concentration and a zeta potential of the order of by -30 mV. We probe nanoparticles either made of maghemite at various particles volume fractions (series based on particles Acit and C) or made of different ferrites (particles D compared to Acit and C). For such dispersions, the local structure has been extensively studied in (Dubois et al. 2000; Gazeau et al. 2002, 2003; Mériguet et al. 2006) in the conditions of [cit]free and Φ of Table 1 both in zero field and under field. In the physicochemical conditions of Table 1, the structure factor is that of a repulsive system as shown in Fig. 2c. These particles can also be dispersed in glycerol or glycerol/water mixtures (sample D_G in Table 1), leading to repulsive interparticle interactions in the conditions of Table 1 (Wandersman et al. 2009a, b).

Note that the samples probed here present no diffraction under field or a very weak diffraction under field therefore no phase separation in two phases under field, phenomenon which gives rise to a very strong characteristic diffraction line. The very weak diffraction line observed in some samples may be indicative of some zero field small aggregates (Avdeev et al. 2009).

Table 2 Samples of series B: acidic ferrofluids of various pH, reached by addition of TMAOH in the sample at pH = 2, $\Phi = 1.5$ %

Sample	pH	$[TAM^+]_{added}$ (mmol/L)	Macroscopic state
B0	2.0	0	Sol of ind. NPs
B1	2.2	3.7	Sol of ind. NPs
B2	2.5	6.8	Sol of ind. NPs
B3	2.6	7.5	Sol of Clusters
B4	3.0	9.0	Sol of Clusters
B5	3.0	9.0	Sol of Clusters
B6	3.3	9.4	Sol of Clusters
B7	3.5	9.7	ThixGel
B8	3.5	9.7	ThixGel
B9	3.7	9.8	ThixGel
B10	3.7	9.8	ThixGel
B11	4.0	9.9	ThixGel
B12	4.2	9.9	ThixGel

Rheological experiments

Development and calibration of magnetorheological cell

Following the specifications detailed in the introduction, our choice concerning a host instrument able to incorporate the development of a specific device for performing rheological experiments under magnetic field lead us to focus on the commercial model MARS II (Thermo Fisher Scientific, USA). This choice is mainly due to the torque control capability, to its sensitivity, and to the convenient geometry with a large space for managing a set of heavy magnetic coils linked to the mechanical surrounding necessary for their accurate and reproducible positioning during the experiments.

The main characteristics of the built device are listed hereunder. Its structure results from the necessity to apply a homogeneous magnetic field to the sample in order to perform significant experiments.

(i)   To fit with the condition of homogeneous field, the simplest solution consists in placing the working plane in the middle of a solenoid of great length. However, the need for a direct access to the samples imposes a structure where the solenoid is split into two parts with, in practice, a narrow interspace left for an access to the working area between these two coils.

(ii) As a consequence, the original working plane of the MARS II system has to be shifted from its bottom position up to the interspace between the twin coils.

(iii) A holder placed inside the lower coil is then necessary to support the working plane (made of titanium) which contains the temperature regulation circuit: either a loop with a stabilized cooling bath, or a Peltier module, linked to a control loop feedback PID (proportional-integral-derivative) controller.

(iv) The interspace gap is used to introduce a space between the coils defining an airtight zone which allows performing experiments under controlled atmosphere and visualizing the samples during their loading and when set in place.

(v)   The upper coil is sustained by a strong mechanical-positioning system needed for up-down and forward-backward movements, allowing the adjustment of both coils positions with or without the spacer present in the gap.

Fig. 2 Structure factor as a function of the scattering vector Q as determined from small-angle X-ray (SAXS) or neutron (SANS) scattering on samples similar to those studied here. **a** *Close symbols* are SAXS data from samples BO, B3, B6, and B9 (case of hydroxo ligands at $\Phi = 1.5\%$); *empty symbols* show SAXS at lower Q's on a sample with $\psi_{dd} = 22$, $d_0 = 8.5$ nm and $\sigma = 0.27$, with $\Phi = 1.45\%$; therefore, its characteristics are rather close to sample B. The legend gives the pH and the concentration of free species. **b** Structure factors S(Q) corresponding to the *empty symbols* of graph (*a*). **c** SANS on a sample with $\psi_{dd} = 32$, $d_0 = 7$ nm and $\sigma = 0.4$ and citrate ligands (similar to series C). Φ values and concentration of free species are indicated in the legend
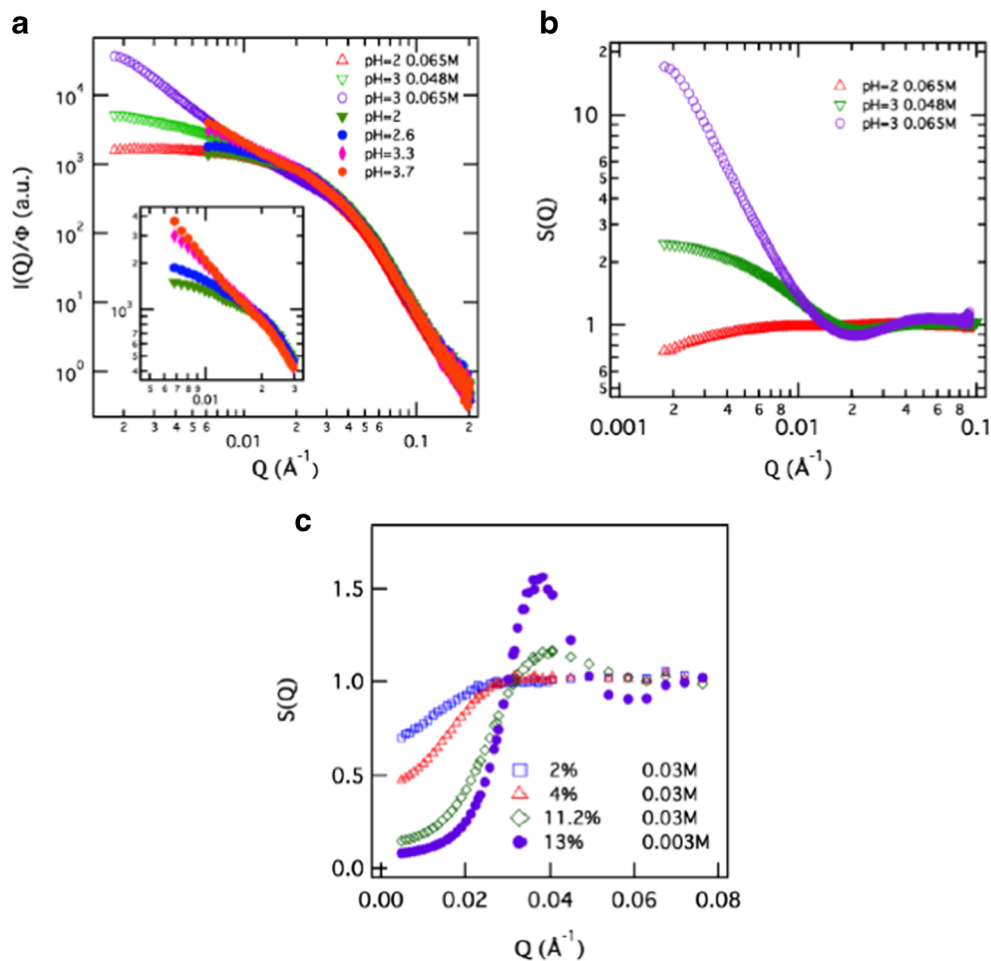
(vi) These air coils have a brass made hollow support, which enables an efficient cooling by means of a water loop (the maximum power dissipation being close to 800 W). The two coils can be placed without any space separation to maximize the field ($H \sim 64$ kA/m) or separated by the spacer in order to see the sample or to fill the cell under gas. In the present study, the coils are separated by a 20-mm spacer so that the maximum field is 31.9 kA/m for 25 A in each coil. The field is thus perpendicular to the shear.

(vii) The tools used for the rheological measurements are the following: a commercial cone (titanium, diameter $D = 59.9$ mm, angle $\theta = 1°$, distance between the truncated cone and the plate in the measurement position of 52 μm) in association with the titanium plane adapted to the top of the holder fixed to the base of the system MARS II inside the lower coil.

(viii) Homogeneity of the magnetic field: two series of determinations of the field are made on the titanium plane surface under several intensities of the applied field at 25.0 ± 0.2 °C. Values are determined using a gauss meter type MG-4D and a Hall probe type HP145 S from Walker Scientific. All measurements are performed along two orthogonal diameters of the titanium plane at the center and in six points (10 mm distance), the last points being at the border of the titanium plane.

In the first series, the gap between coils is set at 20 mm. Intensities applied are 5, 10, 20, and 25 A. In all cases, the field measured is constant at ±2 % inside the central area (40 mm diameter). At the border of the plane, it is decreased by 6 to 10 % in the worst cases. An example, at 25 A imposed, the field in the central area is (44.2 ± 0.6) kA/m and (41.7 ± 2.5) kA/m at the border. In the second series, the gap is reduced to about 4 mm (less deformation and higher intensity of the field in the working area). The results are rather good: for instance at a current of 5 A the field measured is (10.4 ± 0.2) kA/m through the whole surface. At 25 A applied, the field observed in the central area is (53.0 ± 0.2) kA/m with a decrease of 0.4 % at the border of the plane.

Note that there is no residual field measurable on the plane even at times less than 1 s after switching off a long lasting high field in the coils. Also, the 1 kW stabilized power supply which works in the current controlled mode does not introduce any measurable noise, neither using the RMS mode of the Gauss meter, nor by analyzing with an oscilloscope a sampled signal induced in a sensor made of a loop of wires and introduced in the gap between the coils. The high inductance of the coils behaves as a perfect low-pass filter.

With this device (see Fig. 3), several tests are performed to evaluate the temperature regulation. Even using a standard system controlling the temperature of the sample by means of a remote water circulation connected to the titanium plane, the cooling of the coils and the control of the sample temperature are efficient enough so that the temperature on the sample is not disturbed by the changes in the residual thermal radiation of the coils. This point is checked with a non-magnetic standard silicone oil (provided by Thermo

Fig. 3 *Up*: central part of the instrument MARS II equipped with the new system; *down*: preparation step of an experiment under specific atmosphere using the septum on the spacer placed between the coils to control the spreading of the sample. A sketch of the cross section of the magnetorheological cell shows schematically the coils (*1*), the Peltier device to control the temperature of the sample (*2*), the solvent trap (*3*), the cone/plane geometry (*4*), and the lines of the magnetic field
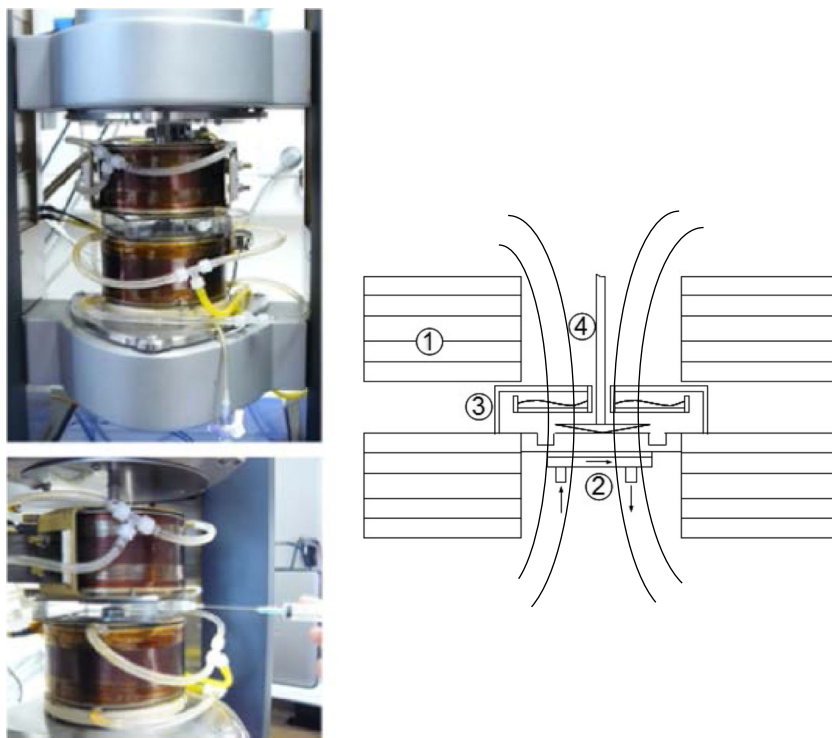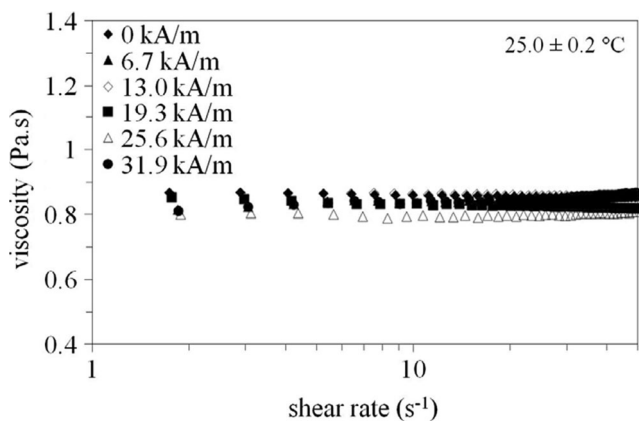
Fig. 4 Viscosity as a function of the shear rate for a viscosity standard based on a non-magnetic silicone oil (at 25 °C) at different magnetic field strengths

Fisher). As shown in Fig. 4, the viscosity as a function of shear rate remains constant as expected for a Newtonian fluid and does not depend on the magnetic field, within the error bar of ± 0.05 Pa.s. The additional specificity of this adapted assembly is the ability to perform measurements under gas in the field thanks to a mechanical system placed inside the upper coil. A liquid seal (water or oil) is mounted on the axis of the rotating cone tool, which makes airtightness inside the region between the plane and the upper coil. Therefore, the samples can also be filled in the rheometer under gas through the space between the coils (Fig. 3), allowing experimentations under a gas flow. Tests made to quantify the influence of this liquid seal on the measurement of very low viscosities show that using pure water the deviation from the reference value appears to be of the same order of magnitude as the resolution level of MARS II system, which depends on the used geometry.

Steady state flow behavior

With the magnetorheological cell, steady shear flow measurements without and with magnetic field are performed by increasing step by step shear rate between 20 and 500 s^{-1} at constant temperature (25.0 ± 0.2)°C. The variable duration of each step is long enough in order to measure stationary values of shear stress and viscosity for different magnetic field strengths for all prepared FFs. With the gel samples of series B at pH $\geq$ 3.5, a pre-shearing of 0.5 Pa during 60 s is applied before starting the measurements.

Results and discussion

The analysis of repulsive systems both without and with magnetic field is first presented. It is followed by the analysis of attractive systems before a generic description of the results in the last part.

Repulsive fluid sols of NPs in zero field

All the samples gathered in Table 1 except samples of series B at pH $\geq$ 2.5 behave as Newtonian fluids in the absence of magnetic field. It confirms that these samples, based on comparable magnetic NPs, present no macroscopic aggregation or phase separation in zero field whatever the mode of stabilization of the sample. The viscosity of the various magnetic fluids increases with the volume fraction as shown in Fig. 5, where the Batchelor's law (Larson 1999) $\eta(H=0)/\eta_{solv} = 1 + 2.5\Phi + 6.2\Phi^2$ accounting at low Φ's for hydrodynamic interparticle interactions of polydisperse hard spheres is plotted for a comparison, the strong increase of viscosity at large volume fractions being due the strong interparticle repulsion at large Φ's.

Repulsive fluid sols of NPs under magnetic field

When a magnetic field is applied, two groups of samples appear, with highly different behaviors depending on the presence or not of small aggregates in the dispersion. A Newtonian behavior is observed in the size-sorted magnetic fluids with a strong interparticle repulsion, while the system behaves as a Bingham fluid under field if some aggregates are still present in the dispersions.

Under field Newtonian magnetic fluids

Four samples, namely samples D, D_G, F, and G (see Tables 1 and 3), remain Newtonian fluids under field. As we wrote above, these fluids present strongly repulsive interparticle interactions in zero field and remain monophasic under field. Moreover, they have been submitted to a size-sorting process by fractional precipitation.
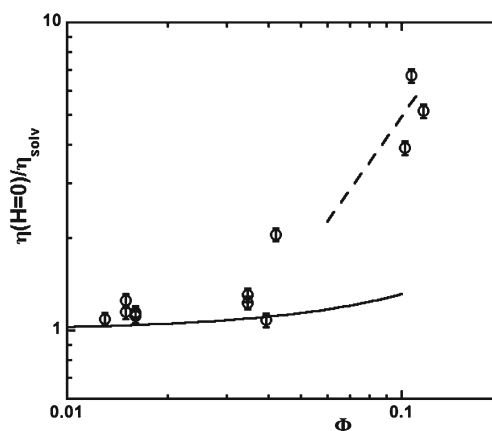
Fig. 5 Log-log representation of zero field relative viscosity at 25 °C as a function of volume fraction Φ for all the samples except samples of series B at pH > 2.5. *Full line* corresponds to development at low Φ for hard spheres (see text). *Dashed line* is a guide for the eye

Table 3 Rheological characteristics of the samples remaining Newtonian under field (see Figs. 5 and 6): η_{solv} is the viscosity of the solvent, η ($H = 0$) is the viscosity of the sample in zero field and η ($H = 31$ kA/m) is the viscosity of the sample under $H = 31$ kA/m

Sample	Φ	η_{solv} (mPas.s)	η ($H = 0$) (mPas.s)	η ($H = 31$ kA/m) (mPas.s)
D	1.3 %	0.9 ± 0.05	0.98 ± 0.05	0.96 ± 0.05
D_G	1.6 %	610 ± 13	687 ± 15	668 ± 15
F	4.2 %	37 ± 1	77 ± 2	90 ± 2
G	11.6 %	19 ± 0.4	96 ± 2	109 ± 2

When the volume fraction is larger than a few percent, the Newtonian viscosity of these samples sensibly increases under field. In these magnetic fluids, a large magnetic field aligns the magnetic moment of the NPs along its own direction and produces a rotation of the NPs body which put their axis of magnetic anisotropy along the applied field. This mechanical orientation of the whole particle induces a subsequent interaction with the flow, and this additional frictional coupling between fluid layers increases the viscosity. This effect decreases as the magnetic energy compared to thermal energy decreases. It has been modelized by M.I. Shliomis (Shliomis 1972) in the limiting case of rigid dipoles (NPs with a rigid coupling between their magnetic moment and their magnetic anisotropy axis). In the present geometry where the applied magnetic field is perpendicular to the local vorticity of the flow, it writes as:

$$\eta_{rel}(H) = \frac{\eta(H)}{\eta(H = 0)} = 1 + \frac{3}{2}\Phi_{Hyd}\frac{\xi - \tanh(\xi)}{\xi + \tanh(\xi)} \qquad (1)$$
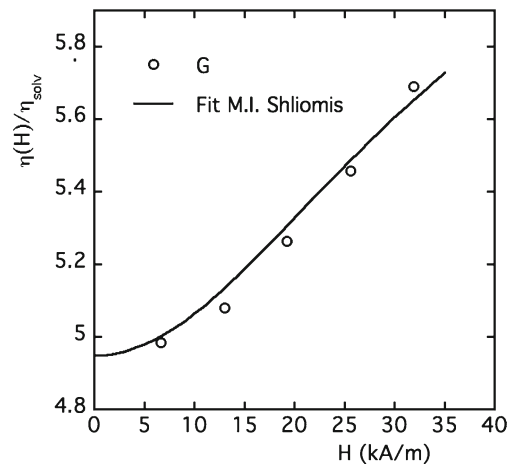
where $\xi = \mu_0\mu H/k_B T$ is the ratio of magnetic energy to thermal energy for a single NP of magnetic moment $\mu = M_S\pi d^3/6$ and Φ_{Hyd} is the hydrodynamic volume fraction of the NPs defined as (Shah et al. 2012):

$$\Phi_{Hyd} = \Phi\left(\frac{d + 2\varepsilon}{d}\right)^3 \qquad (2)$$

ε being the thickness of the surfactant layer.

Fig. 6 Field dependence of the viscosity of sample G, reduced to the solvent viscosity and adjusted with Eq. 1 (*full line*)
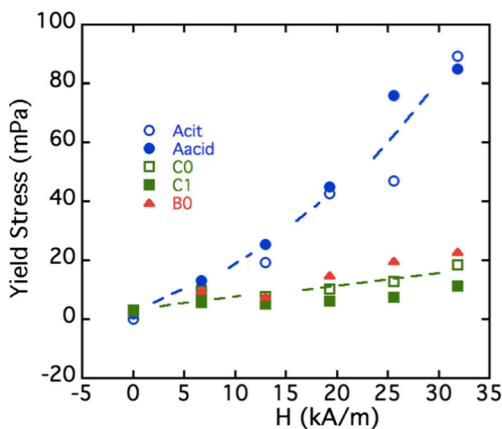
Figure 6 shows the field dependence of $\eta(H)/\eta_{solv}$ for sample G. It is adjusted with Eq. 1 using a volume average of the NP diameter $<d^3>^{1/3} = 10.5$ nm, the NP's magnetisation $M_S = 310$ kA/m and $\Phi_{Hyd} = 2.5$ with $\Phi = 29$ %, associated to a thickness of surfactant layer $\varepsilon = 1.9$ nm, a quite reasonable value for BNE chains.

Under field non-Newtonian magnetic fluids

Under field, all the other fluid samples (samples A, samples of series B at pH $\geq$ 2.5, those of series C) present a shear thinning behavior with a small yield stress and a Newtonian behavior above this yield stress. The flow curves are thus fitted with the Bingham's model:

$$\sigma = \sigma_y + \eta_p\dot{\gamma} \qquad (3)$$

where σ_y is considered as the yield stress and η_p is the plastic viscosity. The plastic viscosity remains for all samples close to the viscosity in zero field $\eta(H = 0)$ plotted in Fig. 5 (see Table 4 discussed further on). On the contrary, the yield stress σ_y depends on the physicochemical parameters as can be seen in Fig. 7, showing its variation with H. In Fig. 7, σ_y values are plotted for three types of particles (A, B, C), two coatings, and low volume fractions ($\Phi < 4$ %). σ_y increases up to 80 mPa at $H = 32$ kA/

Table 4 Non-Newtonian samples under field: volume fraction; concentration of free citrate; zero field viscosity; plastic viscosity determined from the Bingham's fitting of under field flow curves

Sample	Φ (%)	[Cit]$_{free}$ (mol/L)	η ($H = 0$) (mPa.s)	Plastic viscosity (mPa.s)
C0	1.6 %	1.7×10^{-2}	1.01 ± 0.05	1.02 ± 0.05
C1	3.93 %	8×10^{-3}	0.98 ± 0.05	1.03 ± 0.05
A_{cit}	3.47 %	1.3×10^{-2}	1.17 ± 0.05	1.10 ± 0.05
Sample	Φ (%)	pH	η ($H = 0$) (mPa.s)	Plastic viscosity (mPa.s)
A_{acid}	3.47 %	2	1.11 ± 0.05	0.97 ± 0.05
B1	1.5 %	2.2	1.03 ± 0.05	0.90 ± 0.05
B2	1.5 %	2.5	1.12 ± 0.05	0.90 ± 0.05

Fig. 7 Yield stress σ_y as a function of magnetic field H for several samples of Table 4. *Dashed lines* are guides for the eye

m for A_{acid} and A_{cit} while it is much lower for B0, C0, and C1, reaching 20 mPa at $H = 32$ kA/m. It shows that the influence of the coating (hydroxo or citrate ligands), keeping similar ionic strength conditions, here is weak, as well as the influence of volume fraction in this regime. Therefore, the difference of behaviors originates from the size characteristics of the different particles. Indeed, a large σ_y is obtained with particles A for which no size sorting of any kind was performed after the synthesis. A lower σ_y is obtained with particles B and C which have been centrifuged after the synthesis. It means that few small aggregates undetectable in zero field are growing under applied field leading to an increase of σ_y. Eliminating the bigger aggregates by a size-sorting process is thus absolutely determinant to keep Newtonian fluids under magnetic field, as was pointed out in (Shahnazian and Odenbach 2008b). Also, rheological probing can be used to test with a reliable laboratory experiment the presence of aggregates, which can be suspected from diffraction experiments under field. These samples indeed present a very weak diffraction line under field, which is not observed with the other repulsive samples D, D_G, F, and G.

The σ_y determined here are of the same order of magnitude as those obtained by H. Shahnazian et al. [Shahnazian and Odenbach 2007, 2008b) for their tested ferrofluids (typically $\sigma_y \sim 10$ mPa and 45 mPa at $H = 30$ kA/m depending on the proportion of aggregates in the dispersion) and in (Shahnazian et al. 2009) for their fluids based on cobalt nanospheres and nanodiscs stabilized by surfactants in oils. Namely in (Shahnazian et al. 2009) at $H = 30$ kA/m their values σ_y lie between 40 mPa for nanospheres 8 nm in diameter at $\Phi \sim 3$ % and 120 mPa for aggregated nanodiscs 20 nm × 5 nm at $\Phi \sim$ 0.1 %.

Above the yield stress, these under field aggregates are broken by the shear rate and the ferrofluids then flow as simple liquids. Table 4 compares zero field viscosities $\eta(H = 0)$ and under field plastic viscosities $\eta_{plastic}$, as computed by fitting the under field flow curves by Bingham's model (Eq. 3) and averaged over the different H values (as $\eta_{plastic}$ is found to be almost independent of H). They are very close to each other, which can be reasonably explained by the breakage by the flow of the field-induced aggregates. Moreover, they are very close to the viscosity of the water continuous phase ($\eta_{water} = 0.902 \pm 0.003$ mPa.s at 25 °C).

Sols of clusters and thixotropic gels

For the samples of series B at pH ≥ 2.5 (Table 2), the balance of colloidal interactions is attractive due to a decrease of the nanoparticle's surface charge and decrease of interparticle repulsions in this pH range and ionic strength. In these systems, sols of clusters are observed up to pH = 3.3 above which thixotropic gels form. Above pH = 3.3, the time of gelation without magnetic field rapidly increases with pH (Ponton et al. 2005). As illustrated in Fig. 8 for one sol of clusters and one gel, a weak plastic behavior is observed for all samples both without and with magnetic field. A yield stress σ_y is observed, which is H- and pH-dependent for all the samples of
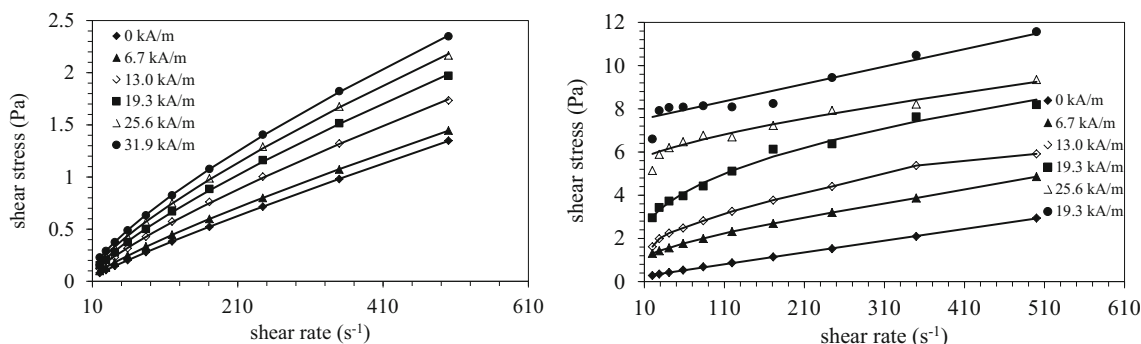
Fig. 8 Shear stress as a function of shear rate at different magnetic field strengths for a sol of cluster (B5, pH = 3.0, *left graph*) and a gel (BII at pH = 4.0, *right figure*). The *solid lines* are fits of the data with Herschel Buckley's model (see Eq. 4)
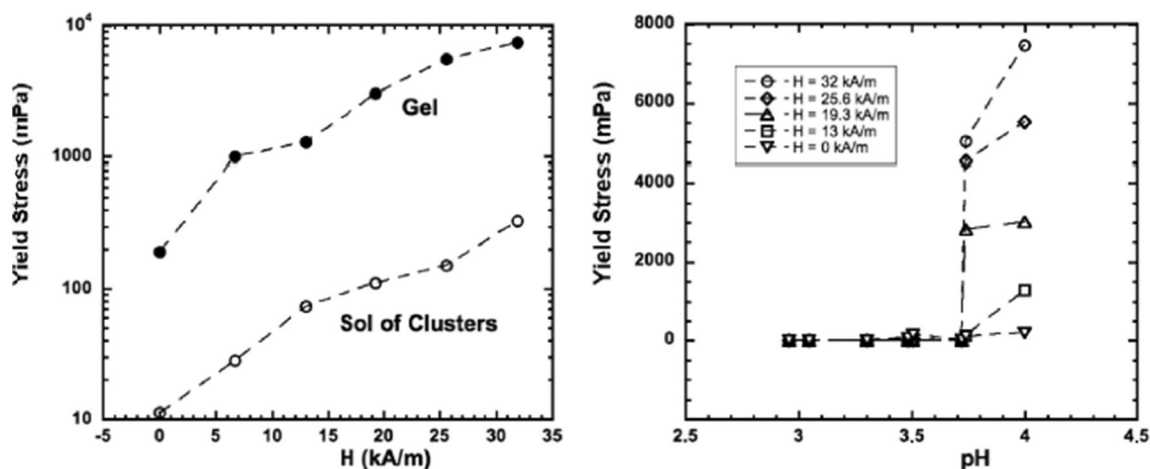
Fig. 9 Yield stress σ_y as a function of applied field H for sol of clusters B3 and thixotropic gel B11 (*left*) and as a function of pH (*right*) for some sols of clusters and gels at different fields H (samples B of Table 2)

series B at $2.6 \leq$ pH ≤ 4.2. Also, the shear stress σ does not increase linearly with the shear rate $\dot{\gamma}$, meaning that under field, the plastic viscosity cannot be defined any-more. This corresponds to a pseudoplastic behavior, and Herschel-Bulckley's model can be used (fits plotted in Fig. 8):

$$\sigma = \sigma_y + K\dot{\gamma}^n \tag{4}$$

where K is the consistency index and n is the shear thin-ning exponent.

The H- and pH-dependences of the yield stress are illus-trated in Fig. 9. Whatever the applied field, the order of mag-nitude of the yield stress in gels (ranging between 10^2 and 10^4 mPa) is much larger than in sols of clusters (of the order of a few 10 mPa). Figure 9 right clearly illustrates the abrupt under field rising of σ_y above pH = 3.5 in the gels. This difference is linked to the aggregation between particles in-duced by the magnetic field. This aggregation is larger when the interparticle interaction becomes less repulsive, which in-creases the yield stress.

The shear thinning exponent n is plotted as a function of magnetic field, for samples of various pH in Fig. 10. The mean value of n for the different pH values at $H = 0$ is 0.86 ± 0.08. These values decrease under applied mag-netic field down to 0.69 ± 0.09 at $H = 32.2$ kA/m as il-lustrated by Fig. 10. This result is consistent with rheo-logical measurements from literature on inverse ferrofluids (Ramos et al. 2011) and on water based Fe_3O_4 ferrofluids stabilized by sodium oleate and PEG (Hong et al. 2009). The experimental values of n always remain between theoretical values (Volkova et al. 2000) predicted for deformation of cylindrical aggregates ($n = 1$) and for chain-like aggregates which rotate before breaking ($n = 2/3$).

The consistency index K, plotted in Fig. 11, increases with the magnetic field strength whatever the pH value due to field-induced aggregation of nanoparticles. However for a constant value of magnetic field, K globally decreases from pH = 3.3 (see Fig. 11). This could be explained by a possible breaking of the thixotropic gels due to the applied pre-shear (0.5 Pa during 60 s).

Flow behavior in terms of magnetic interactions for weakly to strongly clustered samples

For a given state of colloidal interparticle interaction in zero field, the under field flow behavior of magnetic fluids is governed by a balance between magnetic and hydrodynamic forces acting on the nanoparticles. The Mason's number M_n which is defined as the ratio between these hydrodynamic and magnetic forces, appears as a useful reduced number to quantify their respective actions
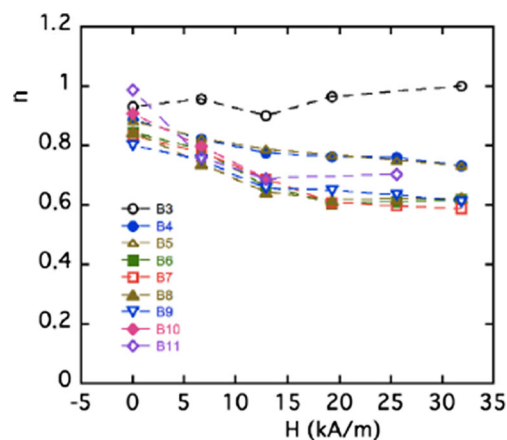
Fig. 10 Shear thinning exponent n as a function of applied field H at different values of pH (sols of clusters and gels—samples B of Table 2)
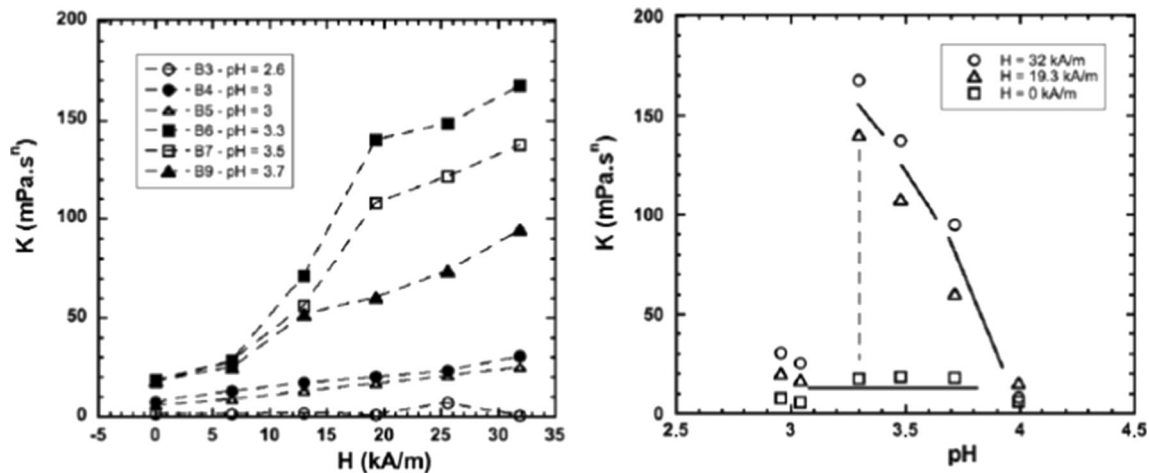
Fig. 11 Consistency index K as a function of applied field H (*left*) and as a function of pH (*right*) for some sols of clusters and gels (samples B of Table 2)
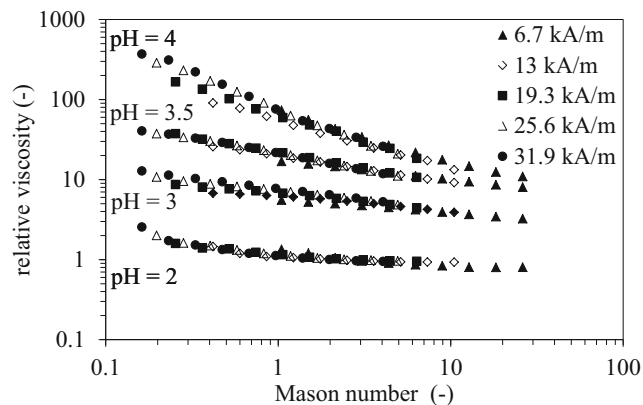
(Soto-Aquino and Rinaldi 2010). This number will be written here for the samples of series B as it is usually written (Santiago-Quinones et al. 2013; Soto-Aquino and Rinaldi 2010) in the case of magnetorheological fluids:

$$M_n = \frac{8\eta_0\gamma}{\mu_0\left(\frac{\mu_{FF}-1}{\mu_{FF}+2}\right)^2 H^2} \quad (5)$$

where η_0 is the viscosity of the solvent, μ_0 is the permeability of vacuum, μ_{FF} is the apparent relative permeability of the ferrofluid. μ_{FF} is obtained by interpolation from the magnetization curves of the ferrofluid through:

$$\mu_{FF} = \frac{M}{H} + 1 \quad (6)$$

Figure 12 presents the variations of the relative viscosity η_{rel} (i.e., shear viscosity divided by solvent viscosity) as a function of Mason's number M_n for several samples of series B at various fields. At $M_n = 10$, the effect of the magnetic field is weak and the probed system is close to the one at $H = 0$. On the contrary, at $M_n \sim 0.15$, the effect of the magnetic field is

dominant. For a given sample at a given pH, the superposition of the curves $\eta_{rel}(M_n)$ is indeed the signature that for this sample the flow behavior is governed by a balance between hydrodynamic and magnetic forces. However a subsidiary dependence of $\eta_{rel}(M_n)$ to physicochemical parameters can be seen in Fig. 12 as different master curves are obtained while pH is increased.

Conclusion

A new magnetorheological cell is designed to investigate the temperature-controlled flow and the viscoelastic properties of complex ferrofluids in a large range of viscosities and yield stresses. In this first study, water-based and oil-based ferrofluids in various states of stabilization are synthesized, characterized, and studied by stationary flow measurements at constant temperature (25.0 ± 0.2 °C) under different magnetic field strengths.

The present investigations explore the influence on rheological properties of the microstructure in home-made samples. In these samples, the interactions between nanoparticles (NPs) are controlled through several parameters. Various soft magnetorheological behaviors are thus encountered here evidencing the determinant role of the following:

– The size-sorting of the NP size distribution able to eliminate nanoaggregates in aqueous solvents,
– An efficient surfaction process of individual NPs in organic solvents,
– The interparticle colloidal interaction, which tunes the microstructure.

They are all of paramount importance for the rheological properties of the magnetic fluids with and without field. The synthesis control parameters allow to finely

Fig. 12 Relative viscosity as a function of Mason' number for several series B samples

tune together both the microstructure and the magnetorheological behavior of the colloidal dispersions resulting, at given colloidal characteristics, from a balance between magnetic and hydrodynamic forces.

The developed device is thus very sensitive and able to probe accurately the various soft magnetorheological behaviors encountered in magnetic fluids with a local structure ranging from NPs individually dispersed with strong interparticle repulsion in aqueous media, with, or without subsidiary aggregates, to nanoparticles aggregated in large clusters or macroscopic thixotropic gels. Forthcoming studies will explore the magnetorheological behavior of more complex magnetic systems, such as mixtures of polymeric solutions with magnetic fluids.

References

Arias JL, Gallardo V, Gomez-Lopera S, Delgado A (2005) Loading of 5-fluorouracil to poly(ethyl-2-cyanoacrylate) nanoparticles with a magnetic core. J Biomed Nanotech 1:214–223

Avdeev MV, Dubois E, Mériguet G, Wandersman E, Garamus VM, Feoktystov AV, Perzynski R (2009) Small-angle neutron scattering analysis of a water-based magnetic fluid with charge stabilization: contrast variation and scattering of polarized neutrons. J Appl Cryst 42:1009–1019

Bacri JC, Perzynski R, Salin D, Servais J (1987) Magnetic transient birefringence of ferrofluids: particle size determination. J Phys France 48:1385–1391

Bacri JC, Perzynski R, Salin D, Cabuil V, Massart R (1989) Phase diagram of an ionic magnetic colloid: experimental study of the effect of ionic strength. J Colloid Interface Sci 132:43–53

Bacri JC, Perzynski R, Salin D, Cabuil V, Massart R (1990) Ionic ferrofluids: a crossing of chemistry and physics. J Magn Magn Mater 85:27–32

Bee A, Massart R, Neveu S (1995) Synthesis of very fine maghemite particles. J of Magn Magn Mater 149:6–9

Berkovski B (1996) ed., Magnetic fluids and applications, Handbook Begell House Inc. Publ. New York

Borin D, Odenbach S (2009) Magnetic measurements on frozen ferrofluids as a method for estimating the magnetoviscous effect. J Phys Condens Matter 21:246002 (5pp)

Cousin F, Cabuil V, Levitz P (2002) Magnetic colloidal particles as probes for the determination of the structure of laponite suspensions. Langmuir 18:1466–1473

Cousin F, Dubois E, Cabuil V (2003) Tuning the interactions of a magnetic colloidal suspension. Phys Rev E 68:021405-1–021405-9

Cruz CD, Sandre O, Cabuil V (2005) Phase behavior of nanoparticles in a thermotropic liquid crystal. J Phys Chem B 109:14292–14299

Dubois E, Cabuil V, Boué F, Perzynski R (1999) Structural analogy between aqueous and oily magnetic fluids. J Chem Phys 111:7147–7160

Dubois E, Perzynski R, Boué F, Cabuil V (2000) Liquid-gas transitions in charged colloidal dispersions: small-angle neutron scattering coupled with phase diagrams of magnetic fluids. Langmuir 16:5617–5625

Duran J, Arias J, Gallardo V, Delgado A (2008) Magnetic colloids as drug vehicles. J Pharm Sci 97:2948–2983

Frka-Petesic B (2010) Ph.D. thesis, UPMC-Paris 6

Frka-Petesic B, Dubois E, Almasy L, Dupuis V, Cousin F, Perzynski R (2013) Structural probing of clusters and gels of self-aggregated magnetic nanoparticles. Magnetohydrodynamics 49:328–338

Galicia A, Cousin F, Dubois E, Sandre O, Cabuil V, Perzynski R (2009) Static and dynamic structural probing of swollen polyacrylamide ferrogels. Soft Matter 5:2614–2624

Galindo-Gonzalez C, de Vicente J, Ramos-Tejada M, Lopez-Lopez M, Gonzalez-Caballero F, Duran J (2005) Preparation and sedimentation behavior in magnetic fields of magnetite-covered clay particles. Langmuir 21:4410–4419

Galindo-Gonzalez C, Lopez-Lopez M, Duran J (2012) J Applied Physics 112:043917-1–043917-11

Gazeau F, Dubois E, Bacri JC, Boué F, Cebers A, Perzynski R (2002) Anisotropy of the structure factor of magnetic fluids under a field probed by small-angle neutron scattering. Phys Rev E 65:031403-1–031403-15

Gazeau F, Boué F, Dubois E, Perzynski R (2003) Static and quasi-elastic small angle neutron scattering on biocompatible ionic ferrofluids: magnetic and hydrodynamic interactions. J Phys Condens Matter 15:S1305–S1334

Gomez-Lopera S, Arias J, Gallardo V, Delgado A (2006) Colloidal stability of magnetite/poly(lactic acid) core/shell nanoparticles. Langmuir 22:2816–2821

Gomez-Ramirez A, Lopez-Lopez M, Duran J (2011) Steady shear flow of magnetic fiber suspensions: theory and comparison with experiments. J Rheol 55:43–68

Hasmonay E, Bée A, Bacri JC, Perzynski R (1999) pH Effect on an ionic ferrofluid: evidence of a thixotropic magnetic phase. J Phys Chem B 103:6421–6428

Hong R, Ren Z, Han Y, Zheng HLY, Ding J (2007) Rheological properties of water-based Fe$_3$O$_4$ ferrofluids. Chem Eng Sci 62:5912–5924

Hong R, Li J, Zhang S, Li H, Zheng Y, Ding J, Wei D (2009) Preparation and characterization of silica-coated Fe3O4 nanoparticles used as precursor of ferrofluids. Appl Surf Sci 255:3485–3492

Huang JP, Wang ZW, Holm C (2005) Computer simulations of the structure of colloidal ferrofluids. Phys Rev E 71:061203-1–061203-11

Itri R, Depeyrot J, Tourinho F, Sousa M (2001) Nanoparticle chain-like formation in electrical double-layered magnetic fluids evidenced by small-angle X-ray scattering. Eur Phys J E 4:201–208

Kroell M, Pridoehl M, Zimmermann L, Pop S, Odenbach S (2005) Magnetic and rheological characterization of novel ferrofluids. J Magn Magn Mater 289:21–24

Kuzhir P, Gomez-Ramirez A, Lopez-Lopez M, Bossis G, Zubarev A (2011) J Non-Newtonian Fluid Mech 166

Larson RG (1999) The structure and rheology of complex fluids, Oxford Univ. Press Inc., N.Y

Lopez-Lopez M, Zugaldia A, Gonzalez-Caballero F, Duran J (2006) Sedimentation and redispersion phenomena in iron-based magnetorheological fluids. J Rheol 50:543–560

Lopez-Lopez M, Zugaldia A, Gomez-Ramirez A, Gonzalez-Caballero F, Duran J (2008) Effect of particle aggregation on the magnetic and magnetorheological properties of magnetic suspensions. J Rheol 52:901–912

Massart R (1980) Preparation of aqueous ferrofluids without using surfactant—behavior as a function of the pH and the counterions. CR Acad Sci Paris Ser C 291:1–3

Massart R (1981) Preparation of aqueous magnetic liquids in alkaline and acidic media. IEEE Trans Magn MAG-17:1247–1248

Mériguet G, Dubois E, Perzynski R (2003) Liquid-liquid phase-transfer of magnetic nanoparticles in organic solvents. J Colloid Interface Sci 267:78–85

Mériguet G, Cousin F, Dubois E, Boué F, Cebers A, Farago B, Perzynski R (2006) What tunes the structural anisotropy of magnetic fluids under a magnetic field. J Phys Chem B 110:4378–4386

Mériguet G, Wandersman E, Dubois E, Cebers A, de Andrade GJ, Demouchy G, Depeyrot J, Robert A, Perzynski R (2012) Magnetohydrodynamics 48:415–426

Mertelj A, Cmok L, Copic M (2009) Anomalous diffusion in ferrofluids. Phys Rev E 79:041402-1–041402-8

Odenbach S, Stork H (1998) Shear dependence of field-induced contributions to the viscosity of magnetic fluids at low shear rates. J Magn Magn Mater 183:188–194

Odenbach S, Rylewicz T, Heyen M (1999) A rheometer dedicated for the investigation of viscoelastic effects in commercial magnetic fluids. J Magn Magn Mater 201:155–158

Park B, Fang F, Choi H (2010) Magnetorheology: materials and application. Soft Matter 6:5246–5253

Patel R (2011) Mechanism of chain formation in nanofluid based MR fluids. J Magn Magn Mater 323:1360–1363

Ponton A, Bée A, Hasmonay E, Perzynski R, Talbot D (2002) Dynamic probing of thixotropic magnetic gels. J Magn Magnc Mater 252:232–234

Ponton A, Bée A, Talbot D, Perzynski R (2005) Regeneration of thixotropic magnetic gels studied by mechanical spectroscopy: the effect of the pH. J Phys Condens Matter 17:821–836

Ramos J, Hidalgo-Alvarez R, de Vicente J (2011) Steady shear magnetorheology of inverse ferrofluids. J Rheol 55:127–152

Ren Z, Han Y, Hong R, Ding J, Li H (2008) On the viscosity of magnetic fluid with low and moderate solid fraction. Particuology 6:191–198

Rodriguez-Arco L, Lopez-Lopez M, Duran J, Zubarev A, Chirikov D (2011) Stability and magnetorheological behaviour of magnetic fluids based on ionic liquids. J Phys Condens Matter 23:455101 (15pp)

Sandre O, Browaeys J, Perzynski R, Bacri JC, Cabuil V, Rosensweig RE (1999) Assembly of microscopic highly magnetic droplets: magnetic alignment versus viscous drag. Phys Rev E 59:1736–1746

Santiago-Quinones DI, Raj K, Rinaldi C (2013) A comparison of the magnetorheology of two ferrofluids with different magnetic field-dependent chaining behavior. Rheol Acta 52:719–726

Shah K, Upadhyay RV, Aswal VK (2012) Influence of large size magnetic particles on the magneto-viscous properties of ferrofluid. Smart Mater Struct 21:075005 (12pp)

Shahnazian H, Odenbach S (2007) Int J Mod Phys B 21:4806–4812

Shahnazian H, Odenbach S (2008a) New driving unit for the direct measurement of yield stress with a stress controlled rheometer. Appl Rheol 18:54974 (7pp)

Shahnazian H, Odenbach S (2008b) Rheological investigations of ferrofluids with a shear stress controlled rheometer. J Phys Condens Matter 20:204137 (4pp)

Shahnazian H, Graf D, Borin D, Odenbach S (2009) Rheology of a ferrofluid based on nanodisc cobalt particles. J Phys D Appl Phys 42:205004 (6pp)

Shima PD, Philip J (2011) Tuning of thermal conductivity and rheology of nanofluids using an external stimulus. J Phys Chem C 115:20097–20104

Shliomis MI (1972) Effective viscosity of magnetic suspensions. Zh Eksp Teor Fiz 61:2411–2418 [Sov Phys JETP 34: 1291-1294]

Soto-Aquino D, Rinaldi C (2010) Magnetoviscosity in dilute ferrofluids from rotational Brownian dynamics simulations. Phys Rev E 82:046310-1–046310-10

Tourinho FA, Franck R, Massart R (1990) Aqueous ferrofluids based on manganese and cobalt ferrites. J Mater Sci 25:3249–3254

Vereda F, de Vicente J, Segovia-Gutierrez J, Hidalgo-Alvarez R (2011) Average particle magnetization as an experimental scaling parameter for the yield stress of dilute magnetorheological fluids. J Phys D Appl Phys 44:425002 (6pp)

Vicente JD, Klingenberg D, Hidalgo-Alvarez R (2011) Magnetorheological fluids: a review. Soft Matter 7:3701–3710

Volkova O, Bossis G, Guyot G, Bashtovoi V, Reks A (2000) Magnetorheology of magnetic holes compared to magnetic particles. J Rheol 44:91–104

Wandersman E, Dubois E, Cousin F, Dupuis V, Mériguet G, Perzynski R, Cebers A (2009a) Relaxation of the field-induced structural anisotropy in a rotating magnetic fluid. EPL 86:10005 (6pp)

Wandersman E, Dupuis V, Dubois E, Perzynski R (2009b) Rotational dynamics and aging in a magnetic colloidal glass. Phys Rev E 80:041504-1–041504-12

Zubarev A, Odenbach S, Fleischer J (2002) Rheological properties of dense ferrofluids. Effect of chain-like aggregates. J Magn Magn Mater 252:241–243